

Vortices, Maximum Growth and the Problem of Finite-Time Singularity Formation

Diego Ayala and Bartosz Protas*

Department of Mathematics and Statistics, McMaster University
Hamilton, Ontario, L8S 4K1, Canada

September 6, 2018

Abstract

In this work we are interested in extreme vortex states leading to the maximum possible growth of palinstrophy in 2D viscous incompressible flows on periodic domains. This study is a part of a broader research effort motivated by the question about the finite-time singularity formation in the 3D Navier-Stokes system and aims at a systematic identification of the most singular flow behaviors. We extend the results reported in Ayala & Protas (2013) where extreme vortex states were found leading to the growth of palinstrophy, both instantaneously and in finite-time, which saturates the estimates obtained with rigorous methods of mathematical analysis. Here we uncover the vortex dynamics mechanisms responsible for such extreme behavior in time-dependent 2D flows. While the maximum palinstrophy growth is achieved at short times, the corresponding long-time evolution is characterized by some nontrivial features, such as vortex scattering events.

Keywords: 2D Navier-Stokes equation, vortex dynamics, maximum growth, palinstrophy, variational optimization

1 Introduction

The research program referred to in this study is motivated by the questions concerning the existence of smooth solutions to the 3D Navier-Stokes system for arbitrarily large times, corresponding to smooth initial data of arbitrary size. To date, smooth solutions have been proved to exist for *finite* times only (Doering 2009), leaving open the possibility of a spontaneous formation of singularities in finite time. We mean by this the loss of regularity of the solution manifested by the “blow-up” of its certain norms. The importance of this problem has been recognized by the Clay Mathematics Institute which identified it as one of the “millennium problems” (Fefferman 2000). There are also analogous questions concerning the existence of smooth solutions to the 3D Euler equation (Bardos & Titi (2007), Gibbon (2008)), as well as

*Email address for correspondence: bprotas@mcmaster.ca

the equations describing quasi-geostrophic flows (Ohkitani & Yamada (1997), Córdoba et al. (2005), Scott (2011)) and magnetohydrodynamic phenomena (Córdoba & Marliani 2000).

It is believed that, should such blow-up occur in finite time, it should be associated with the formation and amplification of small-scale vortex structures. Indeed, a number of different vortex states have been proposed as the initial data for both the Euler system (e.g., Brachet et al. (1983), Pumir & Siggia (1990), Kerr (1993), Pelz (2001), Grafke & Grauer (2012), Orlandi et al. (2012)) and the Navier-Stokes system (e.g., Brachet et al. (1983), Brachet (1991), Orlandi et al. (2012)) which might possibly lead to singularities in finite time, although the computational evidence is in either case not conclusive (Gibbon 2008). As regards probing the flow behavior, in addition to tracking the time evolution of various vorticity norms, some attention has also been given to geometric criteria (Hou (2009), Grafke & Grauer (2012)) and to characterization of the solutions in the complex plane through the width of the analyticity strip (Pauls (2010), Bustamante & Brachet (2012)). All of the aforementioned candidate flows were postulated in a rather ad-hoc fashion based on purely physical arguments. The goal of the research program this study is a part of is to perform search for such extreme vortex structures in a systematic manner using variational methods of mathematical optimization. It is this aspect of bridging the mathematical theory with large-scale computations that distinguishes the present research program, initiated by Lu & Doering (2008), from earlier efforts.

The key observation is that the question about finite-time singularity formation can be rephrased in terms of boundedness of certain norms of the solution. More precisely, if $\mathbf{u}(t, \cdot)$, $t > 0$, is a 3D velocity vector field corresponding to some smooth initial data $\mathbf{u}_0(\cdot) = \mathbf{u}(0, \cdot)$, then it is well-known that the boundedness of the enstrophy $\mathcal{E}(t) := \frac{1}{2} \int_{\Omega} |\nabla \times \mathbf{u}(t, \mathbf{x})|^2 d\Omega$ will guarantee smoothness of the solution up to time t (Lu & Doering 2008). Using methods of functional analysis, the rate of growth of enstrophy can be estimated as

$$\frac{d\mathcal{E}(t)}{dt} < C\mathcal{E}(t)^3, \quad \text{where } C > 0, \quad (1)$$

which, upon integration with respect to time, leads to

$$\mathcal{E}(t) \leq \frac{\mathcal{E}(0)}{\sqrt{1 - 4t \frac{C\mathcal{E}(0)^2}{\nu^3}}}. \quad (2)$$

For brevity, C will hereafter denote a generic positive constant which may assume different numerical values in different instances. We note that upper bound (2), which is the sharpest result of this kind available to date (Doering 2009), blows up in finite time $t^* = \nu^3 / (4C\mathcal{E}(0)^2)$, and, based on this estimate alone, singularity formation cannot be ruled out. The question about the possibility of finite-time blow-up can be thus cast in terms of sharpness of estimate (2) (by ‘‘sharpness’’ we mean existence of solutions which saturate a given inequality bound). Such problems can be studied using variational optimization methods allowing one to find the vortex structures which are the most singular in a suitable sense. Lu & Doering (2008) used this approach to demonstrate that instantaneous estimate (1) is in fact sharp (up to a numerical prefactor). In order to assess sharpness of the finite-time estimate (2), a question which may hold valuable insights concerning the blow-up problem, one would need to solve the following optimization problem

$$\max_{\mathbf{u}_0 \in H^1(\Omega)} \mathcal{E}(T) \quad \text{subject to } \mathcal{E}(0) = \mathcal{E}_0, \quad (3)$$

where $\mathcal{E}_0 > 0$, $T > 0$ are given, $H^1(\Omega)$ is the Sobolev space of functions with square-integrable gradients (Adams & Fournier 2005) and the control variable is the initial data \mathbf{u}_0 . While numerical solution of optimization problem (3) for a broad range of \mathcal{E}_0 and T is a formidable computational task, it appears within reach of modern methods of PDE-constrained optimization and remains the ultimate long-term goal of this research program. Such problems are typically solved using gradient-based methods where the gradient information is determined based on the solution of a suitable adjoint system.

Analogous questions can in fact be also formulated in the case of simpler systems, such as the 1D Burgers and 2D Navier-Stokes equations. It is known that both 1D Burgers and 2D Navier-Stokes systems have solutions which remain smooth for arbitrary times (Kreiss & Lorenz 2004), hence there is no question about their finite-time blow-up. However, for such systems there also exist analytical upper bounds on the growth of various quantities, analogous to (1) and (2), and since they are obtained with similar methods as for the 3D Navier-Stokes system, the questions about their sharpness are in fact quite relevant. Needless to say, the computational tasks arising in the solution of such variational optimization problems in 1D and 2D are much more tractable than in the 3D setting. Hence, from the fundamental perspective, there is a significant interest in studying how sharp the mathematical analysis is in describing the extreme behavior of 1D and 2D flows. While the main interest, especially from the point of view of the singularity formation, is to assess the sharpness of the *finite-time* estimates, they are obtained from the instantaneous estimates which provide upper bounds on the rate of growth of a given quantity at a *fixed* instant of time. We add that, in contrast to 1D and 3D flows, in 2D flows on unbounded or doubly-periodic domains the enstrophy can only decrease and the relevant quadratic quantity is the palinstrophy (which will be formally defined below). The best estimates available for the different problems are summarized in Table 1 in which we indicate whether or not they have been found to be sharp in earlier investigations and also highlight outstanding open questions. Details concerning the derivation of the different estimates can be found in Lu & Doering (2008), Ayala & Protas (2011) and Ayala & Protas (2013).

In the present study we offer a vortex dynamics perspective on the recent results of Ayala & Protas (2013) where it was shown that one of the estimates for the instantaneous rate of growth $d\mathcal{P}/dt$ of the palinstrophy in 2D is in fact saturated by suitably constrained families of vorticity fields. Moreover, in that study it was also demonstrated that when these maximizing vortex states are used as the initial data for the 2D Navier-Stokes system, then the ensuing flow evolution actually saturates the corresponding finite-time estimate. This is an intriguing finding which is at odds with what was observed in Ayala & Protas (2011) in the case of the 1D Burgers equation, and may also be important for the ultimate question concerning the sharpness of 3D finite-time estimate (2). In this investigation we analyze in some detail the structure of the optimal vortex states responsible for such extreme events. The structure of the paper is as follows: in Section 2 we formally state the problem; in the following Section we briefly recall some of the relevant results from Ayala & Protas (2013) concerning the vorticity fields maximizing $d\mathcal{P}/dt$ under different constraints; in Section 4 we analyze the corresponding time evolution for both short and long times; finally, discussion and conclusions are deferred to Section 5.

	BEST ESTIMATE	SHARPNESS
1D Burgers instantaneous	$\frac{d\mathcal{E}}{dt} \leq \frac{3}{2} \left(\frac{1}{\pi^2\nu}\right)^{1/3} \mathcal{E}^{5/3}$	YES (Lu & Doering 2008)
1D Burgers finite-time	$\max_{t \in [0, T]} \mathcal{E}(t) \leq \left[\mathcal{E}_0^{1/3} + \frac{1}{16} \left(\frac{1}{\pi^2\nu}\right)^{4/3} \mathcal{E}_0 \right]^3$	NO (Ayala & Protas 2011)
2D Navier-Stokes instantaneous	$\frac{d\mathcal{P}(t)}{dt} \leq \frac{C_2}{\nu} \mathcal{K}^{1/2} \mathcal{P}^{3/2}$	YES (Ayala & Protas 2013)
2D Navier-Stokes finite-time	$\max_{t > 0} \mathcal{P}(t) \leq \left[\mathcal{P}_0^{1/2} + \frac{C_2}{4\nu^{3/2}} \mathcal{K}_0^{1/2} \mathcal{E}_0 \right]^2$	YES (Ayala & Protas 2013)
3D Navier-Stokes instantaneous	$\frac{d\mathcal{E}(t)}{dt} \leq \frac{27C^2}{32\nu^3} \mathcal{E}(t)^3$	YES (Lu & Doering 2008)
3D Navier-Stokes finite-time	$\mathcal{E}(t) \leq \frac{\mathcal{E}(0)}{\sqrt{1 - 4\frac{C\mathcal{E}(0)^2}{\nu^3}t}}$???

Table 1: Summary of the best estimates available to date for the instantaneous rate of growth and the growth over finite time of enstrophy and palinstrophy in 1D Burgers, 2D and 3D Navier-Stokes systems (we refer the reader to Ayala & Protas (2013) for a more complete version of this table featuring some additional estimates in 2D).

2 Two-Dimensional Navier-Stokes System and the Palinstrophy Growth

We are concerned with the motion of a viscous incompressible fluid on a 2D periodic domain $\Omega = [0, 1] \times [0, 1]$ which is governed by the Navier-Stokes system

$$\frac{\partial \omega}{\partial t} + J(\omega, \psi) = \nu \Delta \omega \quad \text{in } (0, \infty) \times \Omega, \quad (4a)$$

$$-\Delta \psi = \omega \quad \text{in } (0, \infty) \times \Omega, \quad (4b)$$

$$\omega(0) = \omega_0 \quad \text{in } \Omega, \quad (4c)$$

where ψ and ω are, respectively, the streamfunction and (scalar) vorticity, whereas ω_0 is the initial condition. In system (4a)–(4c) ν denotes the kinematic viscosity (assumed fixed and equal to 10^{-3} in all the results presented below), Δ is the Laplacian operator and $J(f, g) := \partial_x f \partial_y g - \partial_y f \partial_x g$, defined for $f, g : \Omega \rightarrow \mathbb{R}$, is the Jacobian determinant. For simplicity, we will work with the streamfunction $\psi(t, \cdot) : \Omega \rightarrow \mathbb{R}$ as the state variable. The following quadratic quantities will play a key role in our analysis

$$\text{kinetic energy} \quad \mathcal{K}(\psi(t)) = \frac{1}{2} \int_{\Omega} |\nabla \psi(t, \mathbf{x})|^2 d\Omega, \quad (5)$$

$$\text{enstrophy} \quad \mathcal{E}(\psi(t)) = \frac{1}{2} \int_{\Omega} (\Delta \psi(t, \mathbf{x}))^2 d\Omega, \quad (6)$$

$$\text{palinstrophy} \quad \mathcal{P}(\psi(t)) = \frac{1}{2} \int_{\Omega} |\nabla \Delta \psi(t, \mathbf{x})|^2 d\Omega. \quad (7)$$

Noting that, for the evolution described by system (4a)–(4c), we always have $d\mathcal{E}(t)/dt = -2\nu\mathcal{P}(t) < 0$, in 2D flows one is interested in the rate of growth of the palinstrophy \mathcal{P} which

can be expressed using Navier-Stokes equation (4a) as

$$\frac{d\mathcal{P}(t)}{dt} = \int_{\Omega} J(\Delta\psi, \psi)\Delta^2\psi d\Omega - \nu \int_{\Omega} (\Delta^2\psi)^2 d\Omega =: \mathcal{R}_{\mathcal{P}}(\psi). \quad (8)$$

Using rigorous methods of mathematical analysis, this quantity can be upper bounded as

$$\frac{d\mathcal{P}}{dt} \leq \frac{C}{\nu} \mathcal{K}_0^{\frac{1}{2}} \mathcal{P}_0^{\frac{3}{2}}, \quad (9)$$

which leads to the following finite-time estimate

$$\max_{t>0} \mathcal{P}(t) \leq \left[\mathcal{P}_0^{1/2} + \frac{C}{4\nu^2} \mathcal{K}_0^{1/2} \mathcal{E}_0 \right]^2 \quad (10)$$

in which $\mathcal{K}_0 := \mathcal{K}(0)$, $\mathcal{E}_0 := \mathcal{E}(0)$ and $\mathcal{P}_0 := \mathcal{P}(0)$. For the derivation of these estimates and a discussion of other bounds on $d\mathcal{P}/dt$ and $\max_{t>0} \mathcal{P}(t)$ the reader is referred to Ayala & Protas (2013). Here we only remark that quantity $\mathcal{R}_{\mathcal{P}}(\psi)$, cf. (8), is intrinsically related to the stretching of the vorticity gradients $\nabla\omega$. As is well-known (see, e.g., Protas et al. (1999)), the equation characterizing the evolution of $\nabla\omega$ features a quadratic stretching term reminiscent of the ‘‘vortex stretching’’ term in the 3D vorticity equation.

3 Vortex States Maximizing the Instantaneous Rate of Growth of Palinstrophy

In order to provide the context for the main results of this paper presented in the next Section, we briefly recall here some of the most important findings from Ayala & Protas (2013) concerning the vortex states maximizing $d\mathcal{P}/dt$, cf. (8). The key question is whether estimate (9) can be saturated by vortex states with prescribed energy \mathcal{K}_0 and palinstrophy \mathcal{P}_0 . To address this question, such maximizing vorticity fields $-\Delta\tilde{\psi}_{\mathcal{K}_0, \mathcal{P}_0}$ were sought via solution of the following constrained optimization problem

$$\begin{aligned} \tilde{\psi}_{\mathcal{K}_0, \mathcal{P}_0} &= \arg \max_{\psi \in \mathcal{S}_{\mathcal{K}_0, \mathcal{P}_0}} \mathcal{R}_{\mathcal{P}_0}(\psi) \\ \mathcal{S}_{\mathcal{K}_0, \mathcal{P}_0} &= \left\{ \psi \in H^4(\Omega) : \frac{1}{2} \int_{\Omega} |\nabla\psi|^2 d\Omega = \mathcal{K}_0, \frac{1}{2} \int_{\Omega} |\nabla\Delta\psi|^2 d\Omega = \mathcal{P}_0 \right\} \end{aligned} \quad (11)$$

(for some technical reasons, maximization is performed in the Sobolev space $H^4(\Omega)$ of functions with square-integrable derivatives of order up to 4 (Adams & Fournier 2005)). We note that the main difficulty in solving problem (11) is the presence of two nonlinear constraints which means that the maximizers $\tilde{\psi}_{\mathcal{K}_0, \mathcal{P}_0}$ need to be found at the intersection of two nonlinear constraint manifolds. We also add that the values of the constraints are linked through a nested Poincaré’s inequality $\mathcal{K}_0 \leq (2\pi)^{-4} \mathcal{P}_0$.

For a fixed energy \mathcal{K}_0 and in the limit of small palinstrophies $\mathcal{P}_0 \rightarrow (2\pi)^4 \mathcal{K}_0$, solutions of optimization problem (11) can in fact be found analytically and turn out to be the eigenfunctions of the Laplacian operator. For intermediate and large values of the palinstrophy the maximizers $\tilde{\psi}_{\mathcal{K}_0, \mathcal{P}_0}$ are found numerically with a discretized gradient flow combining a variational technique for the determination of the gradient of $\mathcal{R}_{\mathcal{P}}(\psi)$ with respect to ψ and a special method to simultaneously enforce the two constraints. As shown in Figure 1, for each value of \mathcal{K}_0 two

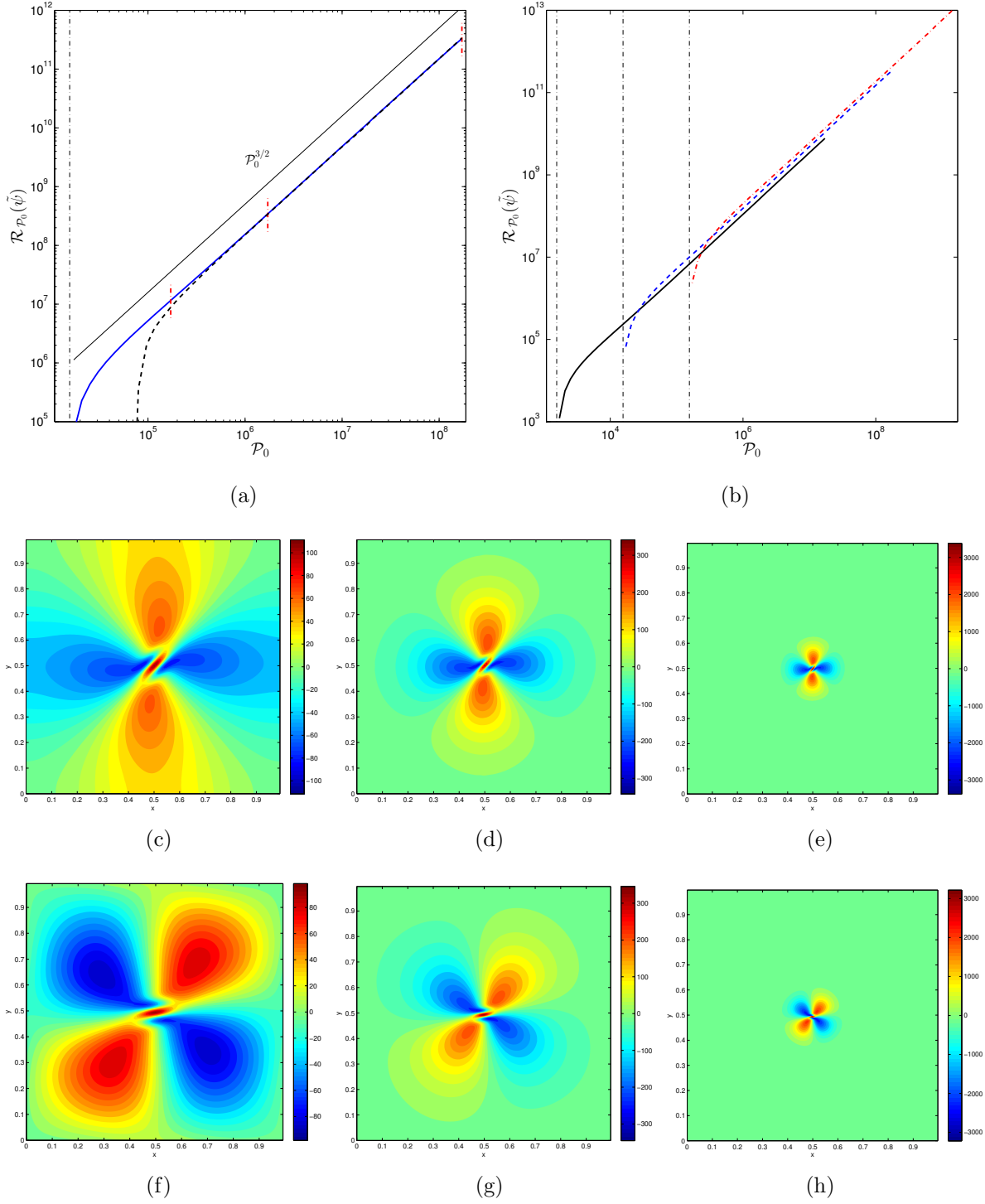


Figure 1: Dependence of the maximum palinstropy rate of growth $\mathcal{R}_{\mathcal{P}_0}(\tilde{\psi}_{\mathcal{K}_0, \mathcal{P}_0})$ on \mathcal{P}_0 for (a) $\mathcal{K}_0 = 10$ and (b) $\mathcal{K}_0 = 10^0$ (solid), $\mathcal{K}_0 = 10^1$ (dashed) and $\mathcal{K}_0 = 10^2$ (dash-dotted). Figure (a) shows two solution branches, whereas figure (b) only the ones with larger values of $\mathcal{R}_{\mathcal{P}_0}$. Optimal vortex states corresponding to the two branches, marked with the solid and dashed lines in figure (a), are shown in figures (c–e) and (f–h), respectively, for the following palinstropy values: (c,f) $\mathcal{P}_0 = 10\mathcal{P}_c$, (d,g) $\mathcal{P}_0 = 10^2\mathcal{P}_c$ and (e,h) $\mathcal{P}_0 = 10^4\mathcal{P}_c$ (marked with short vertical dashes), where $\mathcal{P}_c = (2\pi)^4\mathcal{K}_0$ is the Poincaré limit indicated with vertical dash-dotted lines in figures (a) and (b).

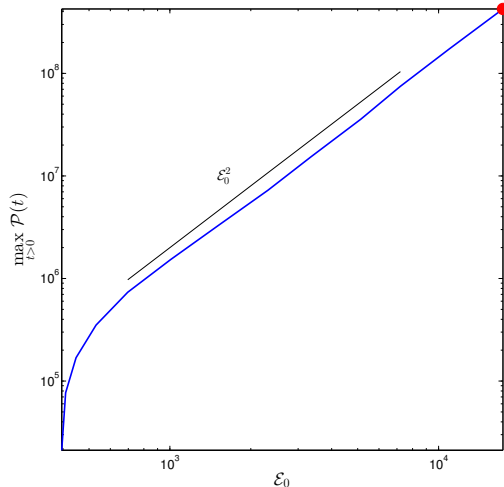


Figure 2: Maximum palinstrophy \mathcal{P}_{\max} as a function of initial enstrophy \mathcal{E}_0 with the optimal vortex states from the upper branch in Figure 1(a) used as the initial data in the solution of Navier-Stokes system (4a)–(4c). Solid symbol (in the top right-hand corner) represents the flow whose time evolution is analyzed in detail in Sections 4.1 and 4.2.

families of maximizing vortex states parameterized by \mathcal{P}_0 were found corresponding to the staggered and aligned arrangement of the vortex cells. We note that in the limit of large \mathcal{P}_0 the rate of growth of palinstrophy characterizing these families exhibits a clear power-law

$$\frac{d\mathcal{P}}{dt} \sim \mathcal{P}_0^{1.49 \pm 0.02} \quad (12)$$

demonstrating that estimate (9) is in fact sharp (up to a numerical prefactor). In other words, the families of vortex states shown in Figures 1(c–h) exhibit the highest rate of palinstrophy production allowed by the mathematical analysis of 2D Navier-Stokes system. An intriguing feature of this family of maximizing vortex states is that, as shown in Figure 2, the time evolution starting from these fields as the initial data (4c) also saturates finite-time estimate (10). Although the maximizing states $\tilde{\psi}_{\mathcal{K}_0, \mathcal{P}_0}$ are obtained with fixed energy \mathcal{K}_0 and palinstrophy \mathcal{P}_0 , cf. (11), to be consistent with the right-hand side of estimate (10), the data in Figure 2 is plotted with the corresponding enstrophy \mathcal{E}_0 on the abscissa. We emphasize that, in contrast to $\tilde{\psi}_{\mathcal{K}_0, \mathcal{P}_0}$, the maximal vortex states obtained under a single constraint on \mathcal{P}_0 , or by fixing \mathcal{E}_0 and \mathcal{P}_0 , *did not* saturate the finite time estimates (Ayala & Protas 2013). Thus, the number and choice of the constraints imposed when solving this type of optimization problems is quite important and deserves further study in the context of the 1D Burgers and 3D Navier-Stokes systems. In the next Section we analyze in detail an example of such an extreme time-evolution of the vorticity field from the family saturating estimate (10).

4 Finite-Time Evolution of Instantaneously Optimal Initial Data

Our main goal in this Section is to identify the physical mechanisms responsible for the growth of the palinstrophy over finite-time intervals which saturates estimate (10). To this end, we select one representative case (marked with a solid symbol) from the family shown in Figure 2 and follow its evolution in time, first over a short-time window (in subsection 4.1) and then over a longer time-window (in subsection 4.2). Navier-Stokes system (4a)–(4c) is solved using $-\Delta\tilde{\psi}_{\mathcal{K}_0, \mathcal{P}_0}$ with $\mathcal{K}_0 = 10$ and $\mathcal{P}_0 = 1.714 \cdot 10^8$ (which correspond to $\mathcal{E}_0 = 1.735 \cdot 10^4$ in Figure 2) as the initial data. While the maximum palinstrophy value \mathcal{P}_{\max} is achieved at short times, the long-time evolution is also shown here as it reveals a number of interesting aspects. The short-time evolution of all cases shown in Figure 2 with \mathcal{E}_0 (or, equivalently, \mathcal{P}_0) sufficiently large follows essentially the same scenario as described below. On the other hand, some details of the long-time evolution may differ between the different cases. Navier-Stokes system (4a)–(4c) is solved numerically with an approach combining a Krylov subspace method for the time discretization with a standard pseudo-spectral technique for the discretization in space. The spatial resolution of 2048^2 ensures that the evolution studied below is well resolved.

4.1 Short-Time Evolution

We analyze here the “stretching event” occurring at the beginning of the time evolution. The history of energy $\mathcal{K}(t)$, enstrophy $\mathcal{E}(t)$ and palinstrophy $\mathcal{P}(t)$ is shown in Figures 3(a,b,c). The snapshots of the vorticity field $\omega(t)$ at some representative instances of time during the event (marked with solid symbols in the plots in Figures 3(a,b,c)) are shown in Figure 4. As discussed in Section 3, the palinstrophy increase ($\mathcal{P}_{\max} - \mathcal{P}_0$) in terms of the initial enstrophy \mathcal{E}_0 is as large as allowed by estimate (10). This increase is clearly visible in Figure 3(c) and, in view of the relation $d\mathcal{E}(t)/dt = -2\nu\mathcal{P}(t)$, is accompanied by accelerated dissipation of the enstrophy visible in Figure 3(b). The evolution of the vorticity field, starting with the instantaneously optimal state $-\Delta\tilde{\psi}_{\mathcal{K}_0, \mathcal{P}_0}$ shown in Figure 4(a), reveals the development of a thin vortex filament stretched by the four satellite vortices. The state when the peak palinstrophy value \mathcal{P}_{\max} is reached is captured in Figure 4(d). After that, the central filament is dissipated and the satellite vortices start to move apart under their own induction as two slightly asymmetric dipoles, see Figure 4(e). An animation showing the short-time evolution of the vorticity field is available on-line as supplementary material.

4.2 Long-Time Evolution

We begin our analysis of the long-time evolution from the final state discussed above. The history of energy $\mathcal{K}(t)$, enstrophy $\mathcal{E}(t)$ and palinstrophy $\mathcal{P}(t)$ is shown in Figures 5(a,b,c), whereas the corresponding vorticity fields are presented in Figure 6. We add that, in order to discount the effect of the vorticity dissipation during the long-time evolution, in Figure 6 we use a different color scale than in Figures 1 and 4. In addition, for clearer presentation of the translating vortices, four copies of the periodic domain Ω are shown in Figure 6. In Figure 7 we also show the trajectories of the four main vortices together with their periodic images (see the Figure caption for the definition of the “vortex cores”). Animations showing the long-time evolution of

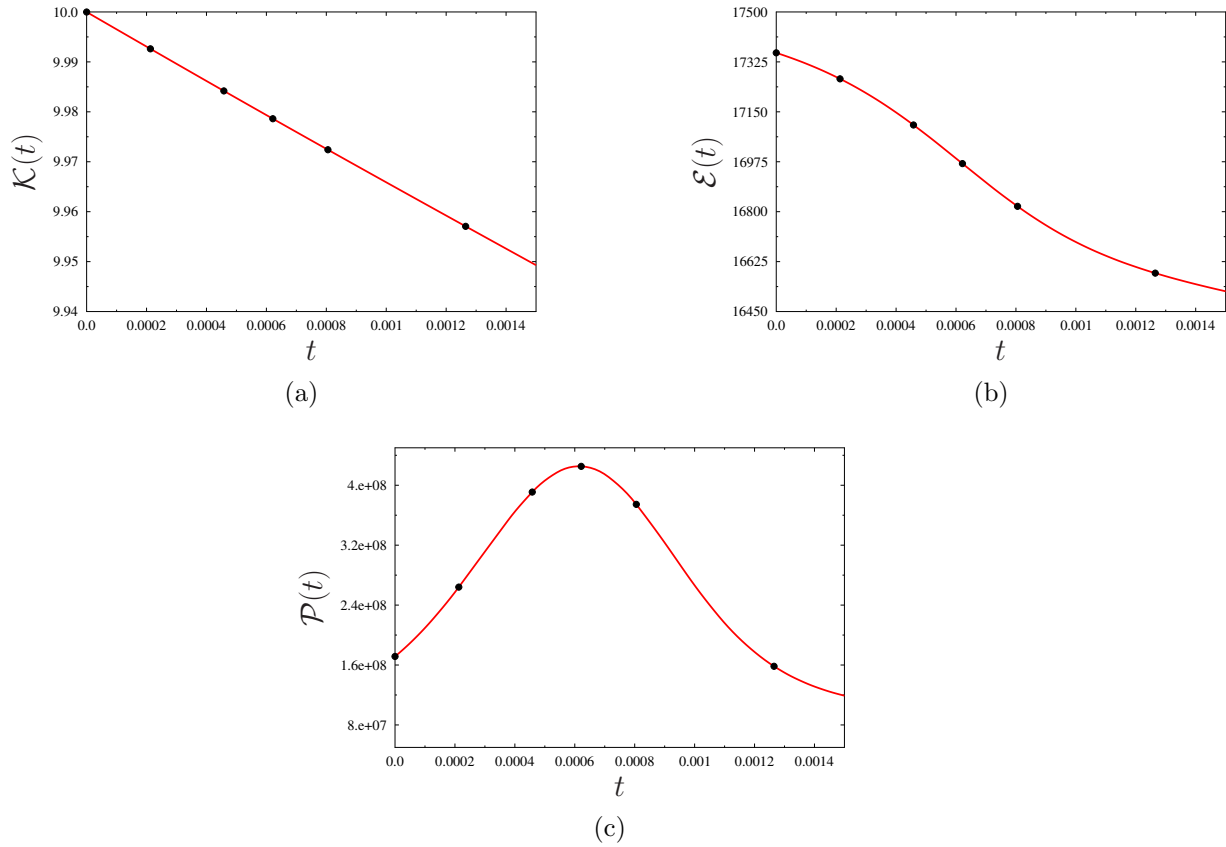


Figure 3: Time histories of (a) energy $\mathcal{K}(t)$, (b) enstrophy $\mathcal{E}(t)$ and (c) palinstrophy $\mathcal{P}(t)$ during an initial stretching event. Solid symbols represent the instances of time for which the vorticity fields are shown in Figure 4.

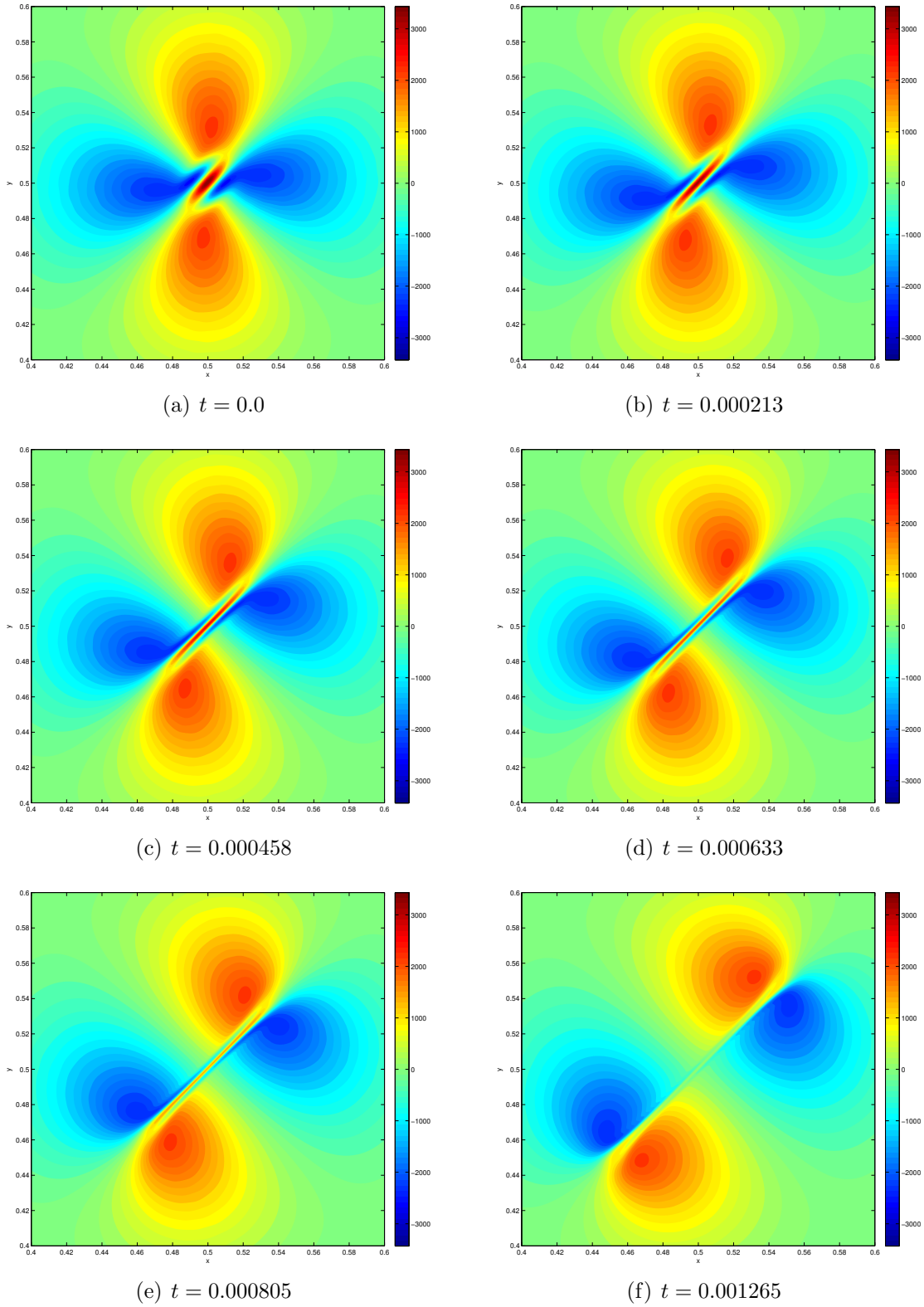
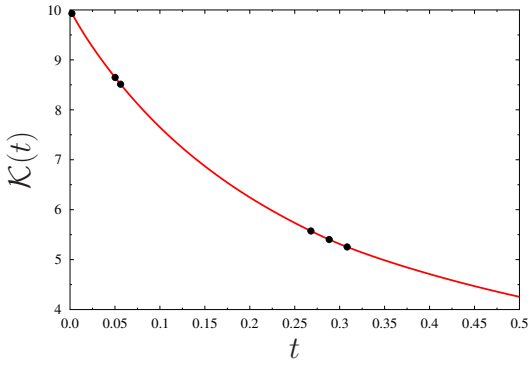
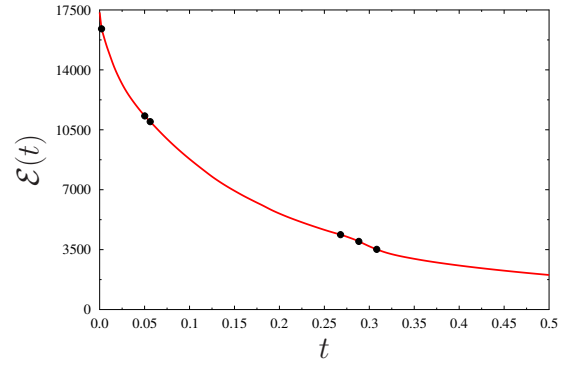


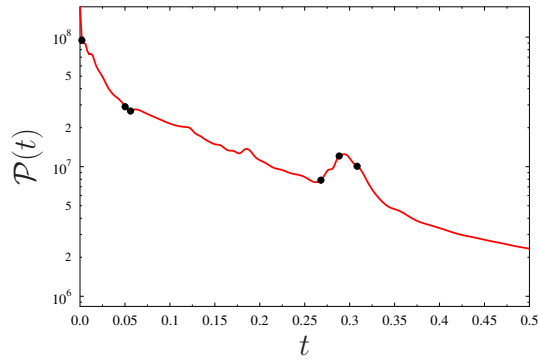
Figure 4: Vorticity fields at the times indicated, and marked with solid symbols in Figures 3(a,b,c), during an initial stretching event. Field (a) is the instantaneously optimal vorticity distribution $-\Delta\tilde{\psi}_{\mathcal{K}_0, \mathcal{P}_0}$, cf. (11), with $\mathcal{K}_0 = 10$ and $\mathcal{P}_0 = 1.714 \cdot 10^8$ used as the initial data (4c) in the Navier-Stokes system.



(a)



(b)



(c)

Figure 5: Time histories of (a) energy $\mathcal{K}(t)$, (b) enstrophy $\mathcal{E}(t)$ and (c) palinstrophy $\mathcal{P}(t)$ during the long-time evolution. Solid symbols represent the instances of time for which the vorticity fields are shown in Figure 6.

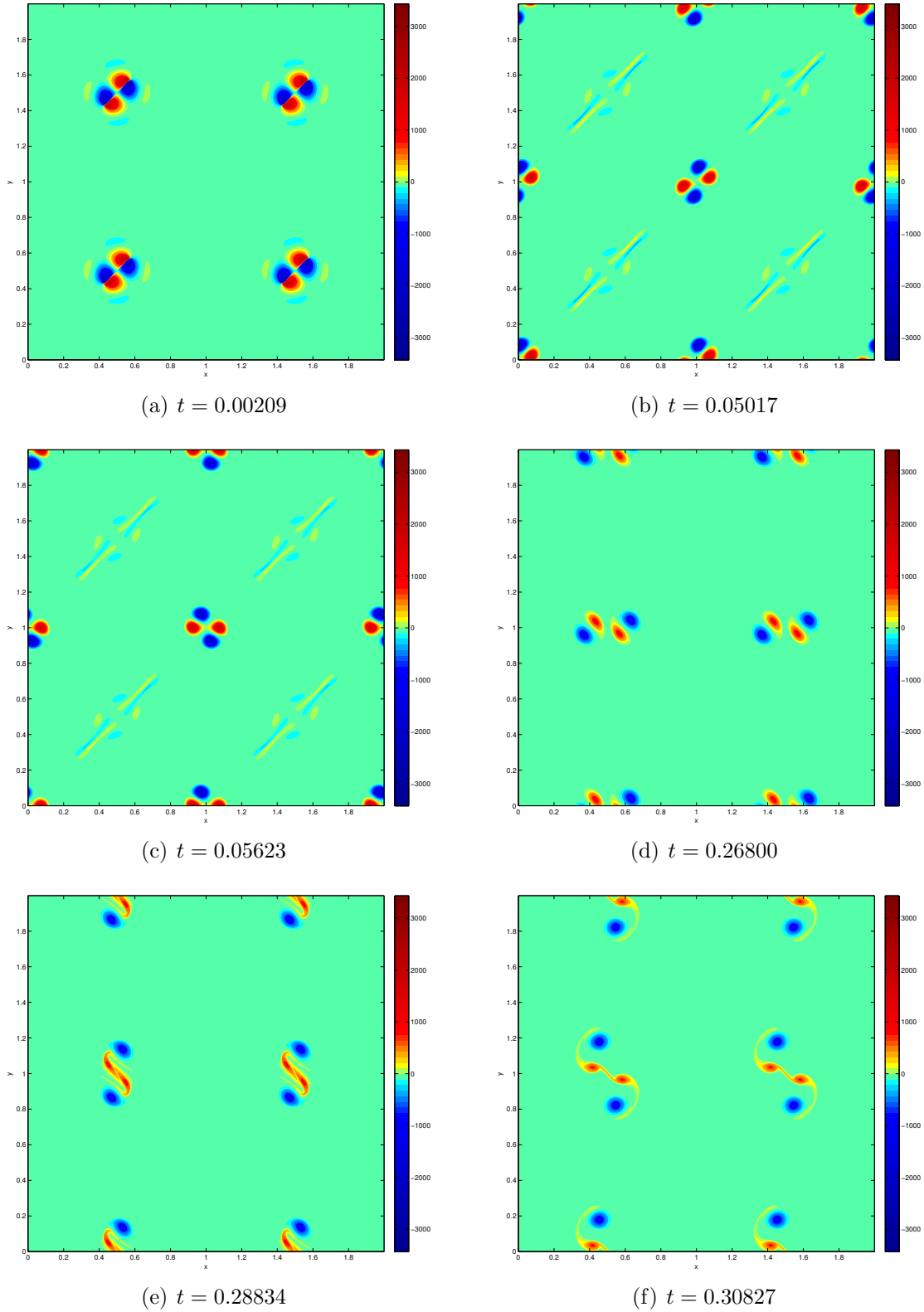


Figure 6: Vorticity fields at the times indicated, and marked with solid symbols in Figures 5(a,b,c), during the long-time evolution. In each Figure four copies of the periodic domain Ω are shown. Field (a) corresponds to the end of the stretching event shown in Figure 4.

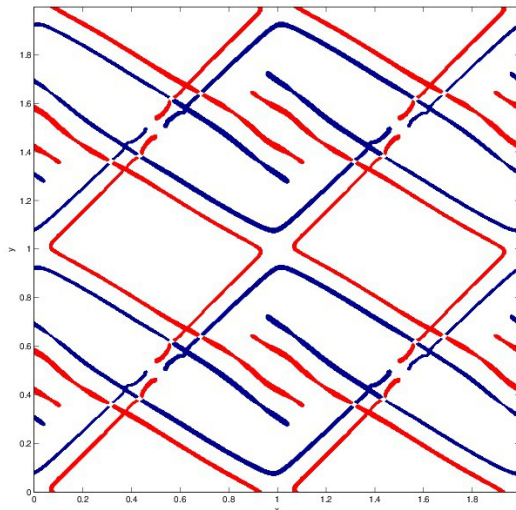


Figure 7: Traces of the vortex cores during the long-time evolution corresponding to the results in Figures 5 and 6. At any given time, the vortex core is defined as the region of the domain Ω where the eigenvalues of the velocity gradient tensor $\nabla\mathbf{u}$ are complex and have magnitude in the range of 90% – 100% of the maximum eigenvalue in the entire domain.

the vorticity field and the trajectories of the vortex cores are available on-line as supplementary material.

Following the initial stretching event discussed in Section 4.1, the vortices move apart as two dipoles to undergo a “scattering event” when they collide and then again move away after exchanging partners (Figures 6(b,c)). As is evident from Figure 5(c), the palinstrophy $\mathcal{P}(t)$ continues to decrease during this event. Its otherwise steady decrease is punctuated by some stretching events occurring later on, such as the event illustrated in Figures 6(d,e,f). The pattern exhibited by the trajectories of the vortex cores shown in Figure 7 is reminiscent of the collision dynamics of pairs of point vortices studied by Eckhardt & Aref (1988). In this regard it should be noted that the present problem is “defective”, in the sense that the vortices making up the dipoles are not identical (cf. Figure 4(f)). This is a result of the asymmetry of the initial optimal configuration $-\Delta\tilde{\psi}_{\mathcal{K}_0, \mathcal{P}_0}$ (Figure 4(a)).

5 Discussion and Conclusions

In this work we have focused on the evolution of the vorticity field starting from the initial data $-\Delta\tilde{\psi}_{\mathcal{K}_0, \mathcal{P}_0}$ which maximizes the instantaneous rate of palinstrophy production $d\mathcal{P}/dt$ under the constraints of fixed energy \mathcal{K}_0 and palinstrophy \mathcal{P}_0 . We identified the physical mechanism leading to the growth of palinstrophy ($\mathcal{P}_{\max} - \mathcal{P}_0$) which in terms of the initial enstrophy \mathcal{E}_0 is as large as allowed by the mathematically rigorous estimate (10). Although here we presented the results for one case only, the stretching mechanism at work at short times is quite robust and was also observed in the short-time evolution corresponding to the initial data $-\Delta\tilde{\psi}_{\mathcal{K}_0, \mathcal{P}_0}$ with different values of \mathcal{K}_0 and \mathcal{P}_0 . On the other hand, details of the long-time evolution could be quite different in these different cases. For example, for some other values of \mathcal{K}_0 and \mathcal{P}_0 , during the scattering event (cf. Figure 6(b,c,d)) the vortices would spin around each other before

moving apart with or without exchanging partners, cf. Eckhardt & Aref (1988). Classifying these different behaviors may be an interesting problem for future research. Another open question is whether the secondary stretching event observed at large times (between $t = 0.25$ and $t = 0.32$) in Figure 5(c), see also Figures 6(d,e,f), saturates bound (9). In order to answer this question, we would need to have data characterizing $d\mathcal{P}/dt$ for some fixed energy \mathcal{K} and the palinstrophy \mathcal{P} varying over some range. Since this stretching event is occurring at large times, there appears to be no easy way to impose these constraints. The long-term interest of the present study is in providing insights about the nature of extreme vortex events which can be useful for addressing similar questions for the flows governed by the 3D Navier-Stokes system.

Acknowledgments

The authors are indebted to Charles Doering and Evelyn Lunasin for many enlightening discussions concerning the research program mentioned in this work. This research was funded through an Early Researcher Award (ERA) and the computational time was made available by SHARCNET.

References

- Adams R A & Fournier J F 2005 *Sobolev Spaces* Elsevier.
- Ayala D & Protas B 2011 On maximum enstrophy growth in a hydrodynamic system *Physica D* **240**, 1553–1563.
- Ayala D & Protas B 2013 Maximum palinstrophy growth in 2D incompressible flows: Instantaneous case. Submitted, see arXiv:1305.7259.
- Bardos C & Titi E S 2007 Euler equations of incompressible ideal fluids *Russ. Math. Surv.* **62**, 409–451.
- Brachet M E 1991 Direct simulation of three-dimensional turbulence in the Taylor–Green vortex *Fluid Dynamics Research* **8**, 1–8.
- Brachet M E, Meiron D I, Orszag S A, Nickel B G, Morf R H & Frisch U 1983 Small-scale structure of the Taylor–Green vortex *Journal of Fluid Mechanics* **130**, 411–452.
- Bustamante M D & Brachet M 2012 Interplay between the Beale-Kato-Majda theorem and the analyticity-strip method to investigate numerically the incompressible Euler singularity problem *Phys. Rev. E* **86**, 066302.
- Córdoba D, Fontelos M A, Mancho A M & Rodrigo J L 2005 Evidence of singularities for a family of contour dynamics equations *PNAS* **102**, 5949–595.
- Cordoba D & Marliani C 2000 Evolution of current sheets and regularity of ideal incompressible magnetic fluids in 2d *Comm. Pure. Appl. Math.* **53**, 512–524.
- Doering C R 2009 The 3D Navier-Stokes problem *Annual Review of Fluid Mechanics* pp. 109–128.

- Eckhardt B & Aref H 1988 Integrable and chaotic motions of four vortices ii. collision dynamics of vortex pairs *Phil. Trans. R. Soc. Lond. A* **326**, 655–696.
- Fefferman C L 2000 ‘Existence and smoothness of the Navier-Stokes equation’ available at http://www.claymath.org/millennium/Navier-Stokes_Equations/navierstokes.pdf. Clay Millennium Prize Problem Description.
- Gibbon J D 2008 The three-dimensional Euler equations: Where do we stand? *Physica D* **237**, 1894–1904.
- Grafke T & Grauer R 2012 Lagrangian and geometric analysis of finite-time Euler singularities. arXiv:1212.0573 [physics.flu-dyn].
- Hou T Y 2009 Blow-up or no blow-up? a unified computational and analytic approach to 3D incompressible Euler and Navier–Stokes equations *Acta Numerica* pp. 277–346.
- Kerr R M 1993 Evidence for a singularity of the three-dimensional, incompressible Euler equations *Phys. Fluids A* **5**, 1725–1746.
- Kreiss H & Lorenz J 2004 *Initial-Boundary Value Problems and the Navier-Stokes Equations* Vol. 47 of *Classics in Applied Mathematics* SIAM.
- Lu L & Doering C R 2008 Limits on enstrophy growth for solutions of the three-dimensional Navier–Stokes equations *Indiana University Mathematics Journal* **57**, 2693–2727.
- Ohkitani K & Yamada M 1997 Inviscid and inviscid-limit behavior of a surface quasigeostrophic flow *Phys. Fluids* **9**, 876–882.
- Orlandi P, Pirozzoli S & Carnevale G F 2012 Vortex events in Euler and Navier-Stokes simulations with smooth initial conditions *Journal of Fluid Mechanics* **690**, 288–320.
- Pauls W 2010 On complex singularities of the 2D Euler equation at short times *Physica D* **329**, 1159–1169.
- Pelz R B 2001 Symmetry and the hydrodynamic blow-up problem *Journal of Fluid Mechanics* **444**, 299–320.
- Protas B, Babiano A & Kevlahan N K R 1999 On geometrical alignment properties of two-dimensional forced turbulence *Physica D* **128**, 169–179.
- Pumir A & Siggia E 1990 Collapsing solutions to the 3D Euler equations *Phys. Fluids A* **2**, 220–241.
- Scott R K 2011 A scenario for finite-time singularity in the quasigeostrophic model *Journal of Fluid Mechanics* **687**, 492–502.